INORGANIC CHEMISTRY FRONTIERS

RESEARCH ARTICLE

View Article Online
View Journal | View Issue

Cite this: *Inorg. Chem. Front.*, 2024, **11**, 6948

Carbon dioxide affinity ("carboxophilicity") of trivalent light metal pyrazolates†

Felix Kracht, Philipp Rolser, Klaus Eichele, Cäcilia Maichle-Mössmer and Reiner Anwander *

Received 2nd July 2024,
Accepted 22nd August 2024

DOI: 10.1039/d4qi01656d

rsc.li/frontiers-inorganic

Trivalent group 3 and 13 light metal pyrazolates were synthesised and their reactivity towards CO_2 was investigated. The homoleptic complex Al(pz^{tBu_2})$_3$ reversibly inserts two molecules of CO_2 to afford Al($CO_2{\cdot}pz^{tBu_2}$)$_2$(pz^{tBu_2}), exhibiting CO_2 release only at elevated temperatures (>100 °C). In contrast, donor-stabilised Sc(pz^{tBu_2})$_3$(thf) forms mono-inserted species [Sc(μ-$CO_2{\cdot}pz^{tBu_2}$)(pz^{tBu_2})$_2$]$_2$, which already releases CO_2 at ambient temperature and pressure and hence is isolable only at low temperature. For the yttrium complex Y(pz^{tBu_2})$_3$(thf)$_2$, insertion of CO_2 is not observable at ambient temperature. The new homoleptic aluminium diisopropyl pyrazolate complex [Al(pz^{iPr_2})$_3$]$_2$ shows exhaustive CO_2 insertion, while dimethyl pyrazolate could be isolated as the separated ion pair [Al(*N*,*N*′,*N*″-Al{pz^{Me_2}}$_3$Me)$_2$][Al(pz^{Me_2})$_3$Me]. The scandium complex Sc(pz^{tBu_2})$_3$(thf) performed best in the catalytic cycloaddition reaction of CO_2 and epoxides, unveiling an inverse correlation of carboxophilicity (=CO_2 affinity) and catalytic activity. Carboxophilicity is assessed using CO_2-release temperature (*via* VT ^{1}H NMR spectroscopy and thermogravimetric analysis).

Introduction

Anthropogenic greenhouse gases, in particular carbon dioxide, are the main reason for global climate change. Consequently, combating CO_2 build-up has developed into the most important and compelling research field in the chemical sciences.[1–11] Carbon dioxide capture and storage (CCS) from flue gas or directly from air (DAC) are industrially realised with aqueous amine scrubbers; this technology, however, is affected by low capacities (<15 wt% CO_2), sensitivity to oxygen and high regeneration energies (high "energy penalty").[8,9] Academic research has focused on amino-functionalized porous materials such as mesoporous silica, zeolites or metal–organic frameworks, with the latter showing promising results under simulated flue gas.[5,12–17] Moreover, a detailed molecular understanding of metal–ligand interactions with carbon dioxide seems crucial for developing efficient (catalytic) processes for its chemical valorization.[18] Here, metal–N(ligand) cooperativity has proven particularly effective in CO_2 transformations together with a synergistic interplay to reversibly insert this heteroallene.[18] Any reversible insertion/de-insertion process will rely on a fine balance of metal-centred oxophilicity and ligand-nitrogen nucleophilicity, which we have termed carboxophilicity (Fig. 1, top).

Recently, we found that CO_2 reversibly inserts into metal–pyrazolato bonds involving oxophilic metal centres. It was revealed that tetravalent dimeric [Ce(pz^{Me_2})$_4$]$_2$ and the trivalent cluster [Ce(pz^{Me_2})$_3$]$_4$ can accommodate 25 wt% CO_2.[19] Adapting this approach to the environmentally friendlier earth-abundant light metal magnesium, parent pyrazolate [Mg(pz)$_2$]$_n$ achieved an exceptionally high reversible CO_2 uptake of up to 35.7 wt%.[20] Structurally authenticated complexes include tetravalent Ce($CO_2{\cdot}pz^{Me_2}$)$_4$ (**A**)[19] and divalent Mg($CO_2{\cdot}pz^{tBu_2}$)$_2$(thf)$_2$ (**B**),[20] showing exclusive κ^2(N,O) carbamato coordination (Fig. 1,

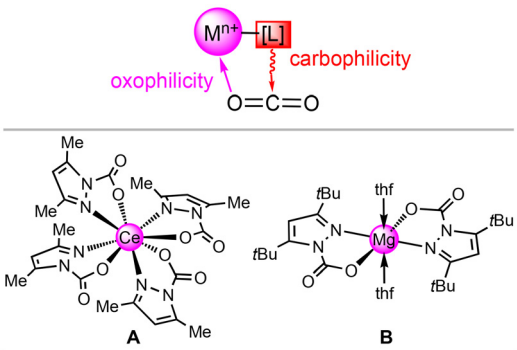

Fig. 1 Top: Carboxophilicity of metal–ligand entities as driven by the oxophilicity of the metal centre and nucleo(carbo)philicity of the ligand. Bottom: Examples of tetravalent (cerium, **A**)[19] and divalent (magnesium, **B**) carbamate complexes,[20] which feature fully reversible CO_2 insertion.

Institut für Anorganische Chemie, Eberhard Karls Universität Tübingen (EKUT), Auf der Morgenstelle 18, 72076, Germany. E-mail: reiner.anwander@uni-tuebingen.de

† Electronic supplementary information (ESI) available. CCDC 2358935–2358943. For ESI and crystallographic data in CIF or other electronic format see DOI: https://doi.org/10.1039/d4qi01656d

bottom). Moreover, all pyrazolate complexes displayed moderate catalytic activity in the conversion of CO_2 and epoxides to their corresponding cyclic carbonates. In this work, we report on the reactivity of trivalent pyrazolates of highly oxophilic group 3 and 13 light metals aluminium, scandium and yttrium towards CO_2. In addition, we discuss CO_2 release temperature as a quantifiable measure for assessing carboxophilicity.

The reactivity of organoaluminium complexes towards carbon dioxide was described by Ziegler in 1960 and expanded on later in 1970 by Weidlein.[21,22] Accordingly, CO_2 inserts irreversibly into trialkyl aluminium compounds to afford tertiary alkoxides or carboxylates, which upon hydrolysis, produced their corresponding alcohols or carboxylic acids. Dimeric $[Al(\mu\text{-}CO_2\cdot N(iPr)_2)(CO_2\cdot N(iPr)_2)_2]_2$ features the first structurally characterised aluminium carbamate complex, accessed from $AlBr_3/HN(iPr)_2/CO_2$.[23] Moreover, dimeric heteroleptic carbamate $[Me_2Al(\mu\text{-}CO_2\cdot N(iPr)_2)]_2$ was obtained (among others) *via* CO_2 insertion into $[Me_2Al(\mu\text{-}N(iPr)_2)_2Mg(\mu\text{-}Me)]_n$.[24] More recently, compound $[Al(\kappa^2\text{-}N,N\text{-}2\{methylamino\}pyridine)_2R]$ (R = Et, iBu) was shown to insert CO_2 not only into the Al–C(alkyl) bond but also in one of the two Al–N bonds of each pyridine ligand.[25,26] Furthermore, the frustrated Lewis acid pair 9,9-dimethylxanthene(PPh_2-$AlMe_2Cl$-AlMeCl) engaged in reversible CO_2 insertion.[27] In addition, aluminium compounds supported by a rigid ligand backbone, such as porphyrinato, salen or amino-tris(phenolato), are active in the cycloaddition of CO_2 with epoxides, with the latter displaying a promising performance with low catalyst loads.[28–36] The porphyrinate complex (TPP)Al(OMe) showed reversible insertion behaviour towards CO_2 in the presence of 1-methylimidazole.[28]

For rare-earth metals, a rich CO_2-insertion chemistry is already existent.[19b] However, for most metal–ligand entities, CO_2 insertion turned out to be irreversible, forming carboxylates/formiate from alkyls/hydrides,[37–42] carbonates from alkoxide/aryloxide[43,44] or carbamates from amide complexes.[45–48] Scandocene $[(C_5Me_5)_2Sc(CO_2\cdot p\text{-tolyl})]$ features the first structurally characterised organoscandium CO_2 insertion complex.[37] Evans *et al.* described the first yttrium carbamate complex, $[(C_5Me_5)_2Y(CO_2\cdot\varepsilon\text{-caprolactam})]_2$, obtained by CO_2 insertion into the Y–N bond of $(C_5Me_5)_2Y(O,N\text{-}\varepsilon\text{-caprolactam})$.[47] Rare-earth-metal complexes also gained attention for their catalytic performance in the co-polymerisation of CO_2 and epoxides to polycarbonates,[43,49–52] as well as the cycloaddition of both compounds to the cyclic carbonates with amino-tris(phenolates) as the most promising catalysts.[52–59] Particularly thanks to the works of the groups of Deacon, Junk, and Winter, there exists a vast variety of rare-earth-metals pyrazolates, featuring distinct coordination modes.[60–64] We were mostly interested in diamagnetic scandium and yttrium pyrazolates, such as $Sc(pz^{tBu_2})_3$,[61] $[Y(pz^{Me_2})_3(thf)]_2$ [62] and $Y(pz^{tBu_2})_3(do)_2$.[60]

Results and discussion

Selection and CO_2 insertion of group 13 pyrazolates

Aluminium pyrazolates. Deacon *et al.* obtained discrete $Al(pz^{tBu_2})_3$ (**1**) *via* a salt-metathesis reaction of $AlCl_3$ and $K(pz^{tBu_2})$ in THF as the first and so far only known homoleptic aluminium pyrazolate complex.[65] In addition to *tert*-butyl-substituted pyrazolate complex **1**, we probed the feasibility of new derivatives bearing smaller, "lighter" methyl and isopropyl substituents. Since the salt-metathesis reactions of $AlCl_3$ and Kpz^{Me_2} led to no isolable product, a protonolysis protocol with $AlMe_3$ and Hpz^{Me_2} was applied. Even though a ratio of 1 : 3 of both compounds was used, only a single methane elimination occurred at ambient temperature, affording the well-known $[Me_2Alpz^{Me_2}]_2$ (**2a**) (Scheme 1).[66,67]

Complex **2a** features a recurring structural motif,[68–70] which was also observed for the new diisopropyl derivative $[Me_2Alpz^{iPr_2}]_2$ (**2b**). Refluxing a 1 : 3 mixture in toluene gave a more extensive but still incomplete ligand exchange. The crystalline material gained overnight revealed the solid-state structure of the separated ion pair $[Al(N,N',N''\text{-}Al\{pz^{Me_2}\}_3Me)_2][MeAl(pz^{Me_2})_3]$ (**3**) (Fig. S102†). The mono-cationic fragment revealed an aluminium(III) centre coordinated by two mono-anionic $[MeAl(pz^{Me_2})_3]^-$ ligands. The latter are reminiscent of the tris(pyrazolyl)hydroborato ligand $Tp^{Me,Me}$, while the Tp analogous aluminium ligand is accessed *via* a protonolysis reaction of $LiAlH_4$ with pyrazole.[71–74] The separated anion in complex **3** is another $[MeAl(pz^{Me_2})_3]^-$ entity. The central aluminium atom of the cationic fragment features a slightly distorted octahedral geometry (N–Al–N angles ±3° off). The aluminium centres of the tridentate "scorpionato"-type ligand adopt a slightly distorted tetrahedral geometry with N–Al–N angles around 100° and C–Al–N angles around 117°. The respective angles in the separated $[MeAl(pz^{Me_2})_3]^-$ anion are 103° and 112° and hence are closer to tetrahedral. The three aluminium centres of the cationic fragment are almost linearly arranged (∠Al, Al, Al 1.5°), with the outer Al1/Al3–N (av. 1.874 Å and 1.893 Å) and inner Al2–N distances (av. 2.035 Å and 2.048 Å) reflecting the distinct coordination numbers. The trinuclear complex $[AlMe(\{N,N'\text{-}3,3'\text{-bipyrazolate}\}_2AlMe_2)_2]$, obtained from bispyrazole and $AlMe_3$ (1 : 1.5),[75] shows a similar structural motif. The ^{27}Al NMR spectrum of compound **3** revealed only two signals at δ = 75.7 ppm and 0.3 ppm, assignable to 4- and 6-coordinated aluminium centres, respectively.

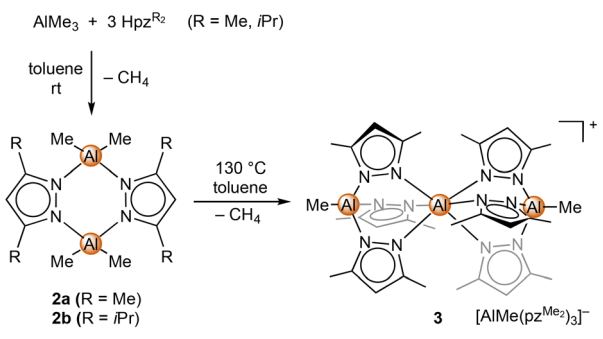

Scheme 1 Protonolysis reactions of $AlMe_3$ with three equivalents Hpz^{R_2} (R = Me and iPr), to form $[Me_2Alpz^{Me_2}]_2$ (**3**) at ambient temperature and separated ion pair $[Al(N,N',N''\text{-}Al\{pz^{Me_2}\}_3Me)_2][MeAl(pz^{Me_2})_3]$ (**4**) by refluxing at 130 °C.

Further heating a 1 : 3 mixture of $AlMe_3$ and Hpz^{Me_2} in mesitylene to 180 °C, in order to achieve full methyl elimination, did not lead to any isolable product, and thus the homoleptic $[Al(pz^{Me_2})_3]$ remains elusive.

Unlike the dimethyl derivative, potassium diisopropyl pyrazolate reacted smoothly with aluminium chloride *via* a salt-metathesis route (Scheme 2). The crystal structure revealed the homoleptic bimetallic complex $[Al(pz^{iPr_2})_3]_2$ (**4**) (Fig. 2), with two bridging pyrazolato ligands arranged in an approximate boat conformation with the aluminium atoms. Interestingly, the terminal pyrazolato ligands show different coordination modes. One aluminium centre features terminal pyrazolatos coordinated exclusively in a κ^1 coordination mode, while the other one accommodates the N-ligand in both κ^1 and κ^2 fashion. The ^1H and ^{13}C NMR spectra of **4** show the bridging and terminal pyrazolatos as two different signal sets in a ratio of 1 : 2. The ^{27}Al NMR resonance was detected at δ = 68.1 ppm. Some reactions gave ^1H NMR spectra with an additional slightly shifted signal set. We were able to fractionally crystallize this side product, and the solid-state structure revealed the monomeric mixed pyrazole/pyrazolato complex $Al(pz^{iPr_2})_3(Hpz^{iPr_2})$ (**4a**) (Fig. S104†). The structure of **4a** is quite similar to that of **4** with one $Al(pz^{iPr_2})_2$ fragment replaced by a proton, which forms a hydrogen bond with the pyrazolyl moieties. Most likely, the pyrazole originated from partial hydrolysis caused by residual moisture in the solvent THF.

Attempts at homoleptic gallium pyrazolates. Since CO_2 insertion/de-insertion into metal–ligand bonds crucially depends on the bond polarization, we also aimed at employing gallium pyrazolates. Surprisingly, homoleptic gallium pyrazolates have not been reported yet.[73,76–79] Given that $[Al(pz^{R2})_3]$ (R = iPr, *t*Bu) could be readily obtained by salt metathesis, we used similar protocols to access putative gallium derivatives. However, the reactions of GaX_3 (X = Cl, Br) with Kpz^{R2} (R = Me, *t*Bu) turned out very unsatisfactorily, and only a small amount of crystalline material could be obtained (Scheme 3).

An X-ray structural analysis revealed the formation of the dimeric complex $[Ga(pz^{tBu_2})(\mu\text{-}N,N,C\text{-}pz^{tBu,C(CH3)2CH2})]_2$ (**5**) (Fig. 3). C–H-bond activation at one *t*Bu moiety under release of pyrazole generated a dianionic pyrazolato ligand, bridging with both nitrogen atoms and one CH_2 group between the gallium atoms.

The molecular structure of complex **5** indicates a rather complex reactivity of gallium pyrazolates. Such distinct behaviour of aluminium and gallium in salt-metathesis reactions is not unknown, as previously shown for $MCl_3/LiN(SiMe_3)_2$ or $MCl_3/LiN(SiHMe_2)_2$ mixtures (M = Al, Ga). There, gallium also engaged in extensive Si–X-bond activation (X = C, H).[80] Application of a protonolysis protocol employing a 1 : 3 mixture of $GaMe_3$ and Hpz^{tBu_2} led to the known $[Me_2Ga$

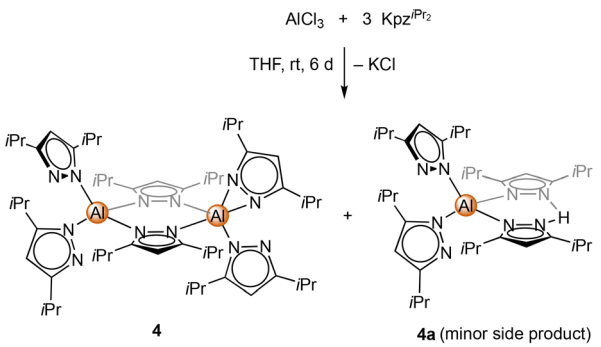

Scheme 2 Synthesis of homoleptic $[Al(pz^{iPr_2})_3]_2$ (**4**) *via* salt metathesis of $AlCl_3$ and Kpz^{iPr_2}. The side product $Al(pz^{iPr_2})_3(Hpz^{iPr_2})$ (**4a**) is formed in the presence of residual moisture.

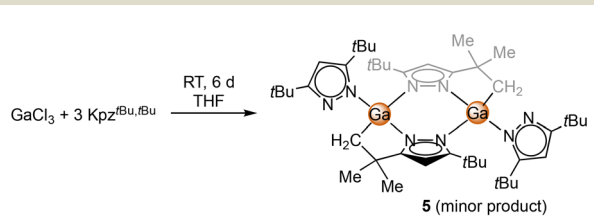

Scheme 3 Reaction of $GaCl_3$ with Kpz^{tBu_2} to yield $[Ga(pz^{tBu_2})(\mu\text{-}N,N,C\text{-}pz^{tBu,C(CH_3)_2CH_2})]_2$ (**5**) as a side product.

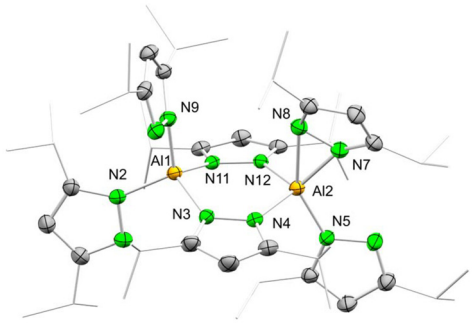

Fig. 2 Crystal structure of $[Al(pz^{iPr_2})_3]_2$ (**4**). Ellipsoids are set at the 50% probability level. Hydrogen atoms are omitted for clarity. See ESI† for selected interatomic distances and angles.

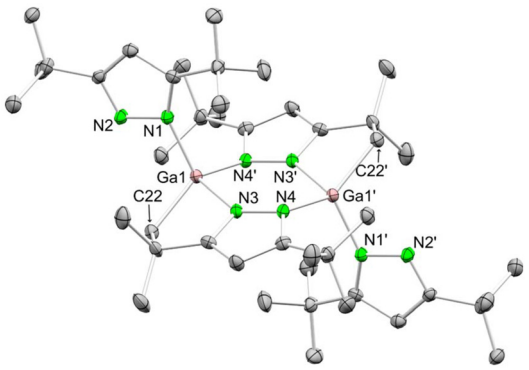

Fig. 3 Crystal structure of $[Ga(pz^{tBu_2})(\mu\text{-}N,N,C\text{-}pz^{tBu,C(CH_3)_2CH_2})]_2$ (**5**). Ellipsoids are set at the 50% probability level. Hydrogen atoms are omitted for clarity. See ESI† for selected interatomic distances and angles.

$(pz^{tBu_2})]_2$,[81] analogous to the aluminium-based reactions displayed in Scheme 1.

Reactivity of aluminium pyrazolates towards CO_2. Reacting Deacon's $Al(pz^{tBu_2})_3$ (**1**) with an excess of CO_2 in THF led to heteroallene insertion into two of the three pyrazolato ligands forming the bis(carbamato) complex $Al(CO_2{\cdot}pz^{tBu_2})_2(pz^{tBu_2})$ (**1-CO_2**) (Scheme 4). The CO_2 content in **1-CO_2** corresponds to 13.5 wt% CO_2 or 3.1 mmol CO_2 per gram. Performing an NMR-scale reaction revealed the formation of a mono-inserted intermediate prior to full conversion into **1-CO_2**. This contrasts with our observations with magnesium and cerium pyrazolates showing such an intermediate only in the CO_2-releasing steps.[19,20]

The crystal structure of **1-CO_2** revealed a strongly distorted octahedral geometry (see Fig. 4). The aluminium centre is coordinated with two carbamato moieties in the κ^2(N,O) mode and one pyrazolato ligand in the terminal κ^2(N,N) mode. Because of the sterically demanding *t*Bu moieties, all three ligands are twisted against each other, which gives the complex a propeller-like overall geometry. Both stereoisomers (Λ,Δ) can be found in the unit-cell which is further corroborated by the centrosymmetric space group *Pbca*. The solid-state structure might also explain the non-occurrence of an exhaustive CO_2 insertion, since the bulky *t*Bu moieties hinder a vital tilt of the third pyrazolato ligand. The inserted CO_2 moieties exhibit an angle around 127.5°, along with localized C–O double (1.199–1.203 Å) and single bonds (1.285–1.288 Å). Such bond localization is also found in the pyrazolato rings. The 4C–3/5C and the 1/2N–3/5C distances of the non-inserted pyrazolato ring differ slightly by 0.005 Å, whereas, for the carbamate pyrazolato rings, the differences are significantly larger at 0.031–0.034 Å and 0.047 Å, respectively.

DRIFTS measurements further validate this behaviour, displaying strong absorption bands at $\tilde{\nu}$ = 1774/1763 cm^{-1} and $\tilde{\nu}$ = 1328 cm^{-1} for the C=O and C–O stretching vibrations, respectively. The ^{1}H NMR spectrum of **1-CO_2** shows two singlets for the pyrazolato backbone proton at δ = 6.32 and 6.00 ppm in a 1 : 2 ratio. Additionally, three singlets with an integral of 18 protons each, one at δ = 1.50 and two at δ = 1.05 ppm, are detected, in accordance with three distinct *t*Bu moieties. Further, the ^{13}C NMR spectrum of **1-CO_2** shows a signal at δ = 146.9 ppm, assignable to inserted CO_2, while the ^{27}Al resonance at δ = 17.0 ppm appears slightly shifted, broadened and less intense (due to loss of symmetry) compared to that of precursor **1** (δ = 23.3 ppm).

Unlike the previously examined cerium and magnesium pyrazolates, solid **1-CO_2** does not show any CO_2 release at ambient temperature, not even under reduced pressure. This high carboxophilicity was further revealed by a variable-temperature (VT) NMR study in THF-d_8 (see S15), revealing prominent CO_2 release only at 90 °C. At this temperature, the formation of small amounts of the mono-inserted complex $[Al(CO_2{\cdot}pz^{tBu_2})(pz^{tBu_2})_2]$ can be detected, while increasing the temperature to 100 °C led to small amounts of **1**. This is in contrast to the CO_2-inserted magnesium pyrazolates which fully de-insert the heteroallene in this temperature range.[19] Cooling the sample which was heated to 100 °C to ambient temperature shows the re-formation of **1-CO_2** as the predominant species, along with small amounts of the mono-inserted complex and **1**. Retreatment of this mixture with an excess of CO_2 fully restores compound **1-CO_2**. A thermogravimetric analysis (TGA) of **1-CO_2** revealed CO_2 release in the temperature range between 114 °C and 196 °C, with a mass loss of 15.8% which is in good agreement with the calculated 13.5%. A single CO_2-release step like in solution could not be observed.

Treatment of $[Al(pz^{iPr_2})_3]_2$ (**4**) with 1 bar CO_2 gave no crystalline material; however, the NMR data suggest an exhaustive insertion into every pyrazolato ligand (see S16–S18†). Three signals for the pyrazolato backbone protons appear in the ^{1}H NMR spectrum in a 1 : 1 : 1 integral ratio. Furthermore, four septets for the tertiary iPr proton are detected in a 3 : 1 : 1 : 1 integral ratio. This indicates the expected asymmetry of the iPr groups resulting from CO_2 insertion, in accordance with distinct signals for the iPr moieties adjacent to the inserted CO_2 and one signal for iPr distant to the inserted CO_2. This assignment is further strengthened by the ^{13}C NMR spectrum, which shows three signals for inserted CO_2 ranging from δ = 147.0 to 146.6 ppm. A ^{1}H–^{13}C HMBC experiment revealed that each of the three pyrazolato backbone proton signals couples with two carbon signals in the shift region for 3/5-pyrazolato carbon atoms, lending more evidence for the new asymmetry. The isopropyl CH_3 groups appear as one multiplet with 24 protons and four doublets with 3 protons. This suggests a hindered

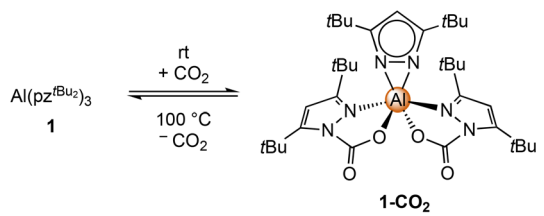

Scheme 4 Reaction of $Al(pz^{tBu_2})_3$ (**1**) with excess CO_2 in toluene.

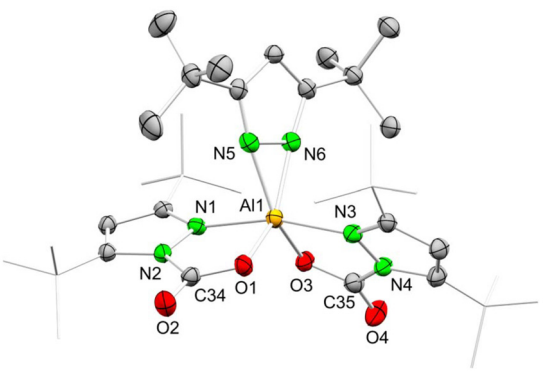

Fig. 4 Crystal structure of $Al(CO_2{\cdot}pz^{tBu_2})_2(pz^{tBu_2})$ (**1-CO_2**). Ellipsoids are set at the 50% probability level. Hydrogen atoms and disorder in the *t*Bu moieties are omitted for clarity. See ESI† for selected interatomic distances and angles.

rotation of the iPr moieties as a result of the three inserted CO_2. Upon CO_2 insertion, the ^{27}Al NMR signal shifted to higher field, from δ = 68.1 ppm in **4** to δ = 12.1 ppm. The putative $[Al(CO_2{\cdot}pz^{iPr_2})_3]$ (**4-CO$_2$**) would infer a capacity of 21.6 wt% CO_2.

Reactivity of group 3 metal pyrazolates towards CO_2

The scandium pyrazolate $Sc(pz^{tBu_2})_3(thf)$ (**7**) was synthesized by applying the salt-metathesis protocol described by Deacon for aluminium pyrazolate $Al(pz^{tBu_2})_3$ (**1**, *vide supra*). Accordingly, the mercury-free synthesis using THF-activated scandium chloride and Kpz^{tBu_2} gave **7** in a good yield (see Scheme 5).

The crystal structure of **7** revealed one THF donor molecule bound to the scandium centre and three κ^2(N,N)-coordinated pyrazolato ligands (see Fig. S107†). Unsurprisingly, the Sc–N distances are slightly longer than those in donor-free $Sc(pz^{tBu_2})_3$.[61] The scope of group 3 metal pyrazolates was extended to the literature known complex $[Y(pz^{Me_2})_3(thf)]_2$ (**9**) obtained *via* protonolysis of YCp_3 with Hpz^{Me2}.[62] Dimeric **9** contains two bridging and four terminal pyrazolato ligands which appear in solution ^1H and ^{13}C NMR experiments as only one signal set due to fast ligand exchange. A ^{13}C CP/MAS NMR experiment revealed separated signal sets for the terminal and bridging ligands (see S26†). The quaternary carbon atoms of the terminal pyrazolatos even appear as four well separated signals. Applying the synthesis protocol as used for scandium complex **7**, monomeric $[Y(pz^{tBu_2})_3(thf)_2]$ (**10**) was obtained. The solid-state structure of **10** revealed two THF donor molecules bound to the metal centre, isostructural to the pyridine-stabilized derivative $[Y(pz^{tBu_2})_3(Py)_2]$ (see S108†).[60]

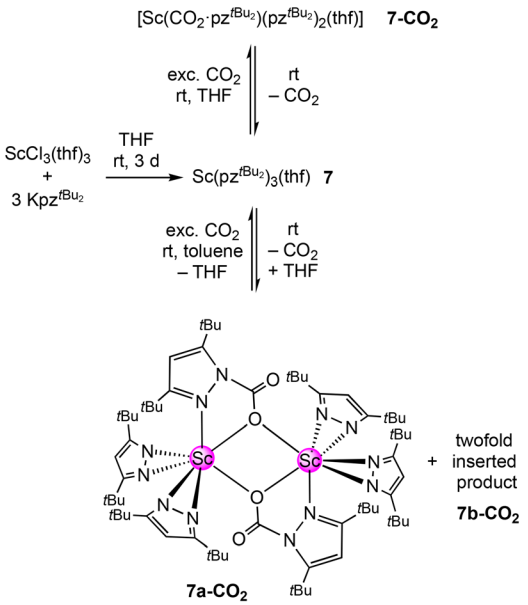

Scheme 5 Salt-metathesis reaction of $ScCl_3(thf)_3$ and Kpz^{tBu_2} to yield donor-stabilised $Sc(pz^{tBu_2})_3(thf)$ (**7**). Treatment with an excess of CO_2 produces the donor-stabilised mono-insertion product $[Sc(CO_2{\cdot}pz^{tBu_2})(pz^{tBu_2})_2(thf)]$ (**7-CO$_2$**) in THF and a mixture of the mono-inserted species $[Sc(CO_2{\cdot}pz^{tBu_2})(pz^{tBu_2})_2]_2$ (**7a-CO$_2$**) and a higher inserted species **7b-CO$_2$** in toluene.

Treatment of $Sc(pz^{tBu_2})_3(thf)$ (**7**) with 1 bar CO_2 in THF-d_8 gave immediate CO_2 insertion, as evidenced by ^1H NMR spectroscopy. Three signals for *t*Bu moieties appeared at δ = 1.51, 1.24 and 0.77 ppm, with an integral ratio of 9 : 36 : 9, respectively, as well as two signals for pyrazolato backbone protons at δ = 6.15 ppm and δ = 6.04 ppm with an integral ratio of 2 : 1, respectively. In addition, two signals of coordinated THF were observed. These signals can be assigned to the mono-inserted donor-stabilized complex $[Sc(CO_2{\cdot}pz^{tBu_2})(pz^{tBu_2})_2(thf)]$ (**7-CO$_2$**). The ^{13}C NMR spectrum shows the resonance for the inserted CO_2 at δ = 149.7 ppm. The CO_2 insertion can be also tracked by ^{45}Sc NMR spectroscopy, since the sharp resonance of **7** at δ = 41.6 ppm shifts slightly towards lower field at δ = 69.1 ppm for **7-CO$_2$**, also involving signal broadening. Unfortunately, we were not able to isolate any crystalline material of **7-CO$_2$**, due to immediate complete CO_2 release in the absence of solvent, already at ambient temperature and pressure. This effective and immediate reversibility of **7**/**7-CO$_2$** is a stark contrast to the aluminium derivative **1-CO$_2$**, where CO_2 release only occurred at elevated temperature and was not observed at reduced pressure. To further confirm CO_2 insertion into scandium pyrazolate **7**, *in situ* DRIFTS experiments were pursued. At 1 bar CO_2 atmosphere, the immediate formation of a single strong band at $\tilde{\nu}$ = 1759 was observed, indicative of a C=O bond stretching vibration (see S98 and S99†). Replacing the carbon dioxide atmosphere by argon resulted in complete CO_2 de-insertion and back-formation of **7**. A VT ^1H NMR experiment uncovered a fully dynamic equilibrium between **7** and **7-CO$_2$** in solution inside a closed vessel (see S31†). Starting with **7-CO$_2$**, even at ambient temperature, traces of **7** were detected. By gradually increasing the temperature, the conversion of **7-CO$_2$** into **7** became more and more prominent and *vice versa*. Cooling the mixture to ambient temperature resulted in an almost identical ^1H NMR spectrum as that at the outset of the VT NMR experiment.

Treatment of **7** with 1 bar CO_2 in toluene-d_8 instead of THF-d_8 resulted in immediate CO_2 insertion as well. However, this time, the ^1H NMR spectrum revealed the formation of two distinct insertion products, **7a-CO$_2$** and **7b-CO$_2$**. One species shows three signals for *t*Bu moieties (9 : 36 : 9) with chemical shifts close to **7-CO$_2$**, while the second species gives four *t*Bu proton signals at δ = 1.69, 1.49, 0.74 and 0.49 ppm with an integral ratio of 18 : 9 : 18 : 9. This second species appeared to be a product with a higher degree of inserted CO_2. Correspondingly, the pyrazolato backbone protons appeared as two sets of two singlets with an integral ratio of 2 : 1. Furthermore, the ^{45}Sc NMR spectrum showed two resonances at δ = 165.7 ppm and δ = 39.1 ppm.

This time, single-crystalline **7a-CO$_2$** could be obtained from the solution; however, like observed for **7-CO$_2$**, solid **7a-CO$_2$** showed immediate CO_2 release at ambient temperature. Therefore, permanent cooling at −40 °C was essential for setting up and performing a successful XRD measurement. The crystal structure revealed the dimeric donor-free mono-

inserted species $[Sc(CO_2{\cdot}pz^{tBu_2})(pz^{tBu_2})_2]_2$ (**7a-CO_2**) bearing the two carbamato ligands in a [μ-1κ^2(N,O):2κ(O)] bridging fashion (Fig. 5). Moreover, the scandium centres accommodate two terminal κ^2(N,N′) pyrazolatos. As indicated by the ^{1}H NMR spectrum, coordinated THF from the starting material was displaced.

The overall reversibility of the CO_2 insertion of **7a-CO_2** is akin to that of **7-CO_2**. The original NMR solution as well as isolated **7a-CO_2** redissolved in toluene-d_8, giving similar ^{1}H NMR spectra, both showing small amounts of the second species **7b-CO_2**. In the absence of a CO_2 atmosphere, **7b-CO_2** seems to be unstable in solution at ambient pressure, which is why no crystalline **7b-CO_2** could be isolated. Given the *t*Bu proton signal set (integral ratio of 18 : 9 : 18 : 9), representing two carbamato ligands and one pyrazolato ligand, species **7b-CO_2** likely features the twofold CO_2-inserted compound $[Sc(CO_2{\cdot}pz^{tBu_2})_2(pz^{tBu_2})]$.

Our attempts to synthesize the homoleptic scandium dimethyl pyrazolate *via* a salt-metathesis protocol [$ScCl_3(thf)_3$ + $3Kpz^{Me_2}$] were unsuccessful. However, on one occasion, the trimetallic oxo-centred cluster $[Sc_3O(pz^{Me_2})_7(Hpz^{Me_2})_2]$ (**8**) was obtained as the main product in a crystalline yield of 74% (see Scheme 6, Fig. 6).[82]

Two scandium centres in **8** are coordinated by four pyrazolato ligands each, and one is coordinated by three pyrazolatos and two donor pyrazoles. Each scandium centre bears one terminal κ^2(N,N′) pyrazolato ligand, while two scandium centres are bridged twice by μ-1κ(N):2κ(N′) pyrazolatos. The scandium centre being single-bridged to the other two accommodates the two pyrazole donors. Overall, a total of one equivalent H_2O is formally required to yield complex **8**, which most likely originated from residual water in the solvent THF.

The ^{1}H NMR spectrum of compound **8** displays the methyl groups and the backbone protons of the pyrazolato and pyrazole ligands as one signal each, at δ = 2.13 ppm and δ = 5.73 ppm, respectively, which indicates rapid exchange of the ligands in solution. The two NH-protons appear as one broad signal at δ = 11.82 ppm. As expected, the ^{45}Sc NMR spectrum features two resonances at δ = 153.2 ppm and δ = 45.1 ppm in a ratio of 1 : 2. More surprisingly, treatment of **8** with 1 bar CO_2 led to two well-defined products as suggested by NMR spectroscopy. One product presents the carbamic acid $HO_2Cpz^{Me_2}$ with typically broad proton and carbon signals, which we reported lately as a co-product of the reaction of mixed pyrazolato/pyrazole magnesium complexes with CO_2 or as a hydrolysis product of the carbamate complexes.[20] The second product **8-CO_2** appeared as three sharp signals in the ^{1}H NMR spectrum at δ = 5.95, 2.26 and 2.18 ppm. This pattern indicates exhaustive CO_2 insertion into the oxo-cluster. This is further implied by the ^{45}Sc NMR spectrum, featuring only one signal at δ = 53.6 ppm. The ^{13}C NMR spectrum revealed two signals for inserted CO_2 at δ = 151.2 ppm and δ = 150.2 ppm, assignable to the carbamic acid and the CO_2-functionalized oxo cluster, respectively. However, no crystalline material of **8-CO_2** could be obtained yet, and attempts to reproduce **8** by using an equimolar amount of water in the reaction depicted in Scheme 5 were unsuccessful.

The CO_2-inserted product of $[Y(pz^{Me_2})_3(thf)]_2$ (**9**) shows the typical splitting of the methyl groups in the ^{1}H NMR spectrum (THF-d_8), resonating at δ = 2.18 ppm and δ = 2.09 ppm, indica-

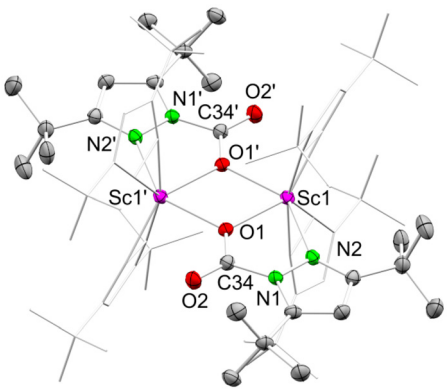

Fig. 5 Crystal structure of $[Sc(CO_2{\cdot}pz^{tBu_2})(pz^{tBu_2})_2]_2$ (**7a-CO_2**). Ellipsoids are set at the 50% probability level. Hydrogen atoms and disorder in the *t*Bu moieties are omitted for clarity. See ESI† for selected interatomic distances and angles.

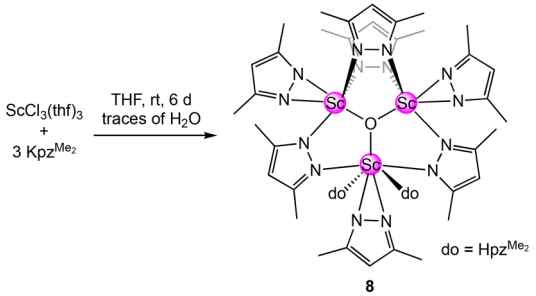

Scheme 6 Synthesis of the oxo-centred cluster $[Sc_3O(pz^{Me_2})_7(Hpz^{Me_2})_2]$ (**8**).

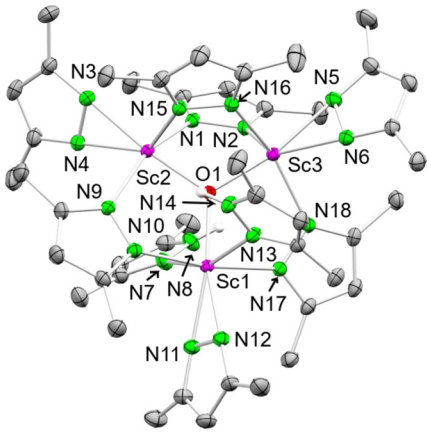

Fig. 6 Crystal structure of $[Sc_3O(pz^{Me_2})_7(Hpz^{Me_2})_2]$ (**8**). Ellipsoids are set at the 50% probability level. Hydrogen atoms are omitted for clarity. See ESI† for selected interatomic distances and angles.

tive of the formation of $Y(CO_2{\cdot}pz^{Me_2})_3(thf)$ (**9-CO$_2$**). However, several other non-assignable signals were detected along with that of putative **9-CO$_2$** (see Fig. S45†), most likely representing a rather complex cluster species. A VT ^{1}H NMR study revealed that **9-CO$_2$** fully back-converts into **9** at 70 °C, while the unknown species remains unchanged (see Fig. S48†). Recently, we introduced a solvent-free procedure, in which the pyrazolate compound is reacted with CO_2 neat as a solid.[20] By using this procedure for **9**, the resulting **9-CO$_2$** exhibited a mass gain of 15.6 wt%. This is slightly higher than the expected value for a two-fold insertion (14.5 wt%) and lower than that for a complete insertion (20.3 wt%). Correspondingly, the ^{13}C CP/MAS spectrum of **9-CO$_2$** revealed two signal sets. One can be assigned to unreacted **9** and the other to putative **9-CO$_2$**. The chemical shifts are comparable to those observed for $[Mg(CO_2{\cdot}pz^{Me_2})_2]_n$ with a resolved signal for inserted CO_2 at 152.1 ppm. A final statement on the amount of inserted CO_2 in **9-CO$_2$** cannot be made. In contrast, $Y(pz^{tBu_2})_3(thf)_2$ (**10**) did not show any traceable CO_2 insertion into the Y–N bond at ambient temperature. Only traces of the carbamic acid $HO_2Cpz^{tBu_2}$ could be detected in the ^{1}H NMR spectrum, pointing to some Hpz^{tBu_2} impurities in **10** (see Fig. S51†). Overall, this indicates that yttrium complex **10** has an even less pronounced capability to bind CO_2 than the scandium congener **7**. This is also in agreement with the CO_2-insertion capability of homoleptic ceric pyrazolates $Ce(pz^{RR'})_4$ which was found to decrease in the order of $pz^{Me2} > pz^{tBu,Me} > pz^{Ph_2} > pz^{tBu_2}$.[83]

Synthesis and reactivity of unsubstituted "parent" pyrazolates of aluminium and scandium

Since the parent pyrazolate $[Mg(pz)_2]_n$ displayed an exceptionally high reversible CO_2 uptake of up to 35.7 wt%,[20] it was of interest to examine such reaction behaviour for the trivalent light metals. The trivalent parent pyrazolates $[Al(pz)_3]_n$ (**11**) and $[Sc(pz)_3]_n$ (**12**) were accessed *via* transamination of $Al(pz^{tBu_2})_3$ (**1**) and $Sc(pz^{tBu_2})_3(thf)$ (**7**) with Hpz in toluene, as indicated by the instant formation of a white precipitate. The ^{13}C CP/MAS spectra of amorphous **11** and **12** showed the expected signal sets (Fig. S52/S54†). The ^{27}Al CP/MAS experiment revealed a signal at 5.2 ppm (Fig. S53†) featuring the most high-field shifted signal observed for a homoleptic aluminium pyrazolate. For polymeric **12**, the ^{45}Sc resonance was resolved at 156.0 ppm (Fig. S55†). Not unexpectedly, the CO_2-uptake behaviours of **11** and **12** were in line with those of the discrete substituted pyrazolates (*vide supra*). When exposing the solids in a very simple manner to an atmosphere of 1 bar CO_2 for three hours, mass gains of 8.2 wt% for **11** and 6.9 wt% for **12** were found. However, these materials rapidly release CO_2 at atmospheric pressure, as indicated by FTIR spectroscopy.

Catalytic cycloaddition of epoxides and CO$_2$

Given our previous works on metal pyrazolates, we were interested in the behaviour of trivalent metal pyrazolates as catalysts in the cycloaddition of epoxides and CO_2 (Table 1). Applying the standard protocol (0.5 mol% catalyst, 1 mol% cocatalyst tetra-*n*-butylammonium bromide (TBAB), epoxide as solvent), the catalysis was performed under 1 bar CO_2 at ambient temperature. After 24 h, the conversion was determined from the ^{1}H NMR spectra. Pyrazolates $Al(pz^{tBu_2})_3$ (**1**) $[Al(pz^{iPr_2})_3]_2$ (**4**), $Sc(pz^{tBu_2})_3(thf)$ (**7**), $[Y(pz^{Me_2})_3(thf)]_2$ (**9**) and $Y(pz^{tBu_2})_3(thf)_2$ (**10**) were employed as catalysts in addition to tetrametallic cluster $[Ce(pz^{Me_2})_3]_4$ (**13**) and the tetravalent $[Ce(pz^{Me_2})_4]_2$ (**14**) for comparison. Propylene oxide, styrene oxide, 2-*tert*-butyloxirane and 1,2-epoxyhexane were employed as substrates. Aluminium complex **1** showed only moderate catalytic activity, converting 65% of propylene oxide to the cyclic carbonate (entry 1). The sterically more demanding epoxides were only minimally converted by complex **1**, which achieved the highest conversion for 1,2-epoxyhexane (7%).

Table 1 Catalytic activities of trivalent metal pyrazolates in the conversion of epoxides to cyclic carbonates[a,b]

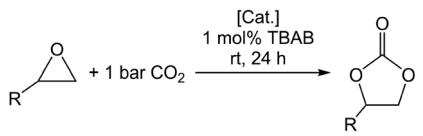

Entry	Catalyst	R = Me	R = Ph	R = *t*Bu	R = *n*Bu
1	**1-Al**	65%	5%	2%	7%
2	**4-Al**	43%	8%	3%	11%
3	**7-Sc**	>99%	27%	24%	29%
4	**9-Y**	84%	20%	5%	22%
5	**10-Y**	97%	22%	8%	18%
6	**13-Ce^{III}**	96%	13%	5%	9%
7	**14-Ce^{IV}**	88%	23%	13%	25%

[a] Reaction conditions: 1 bar CO_2, 0.5 mol% metal centre of the catalyst, 1 mol% TBAB at ambient temperature for 24 h. [b] Conversion determined by comparison of the integral protons at the α-position of the epoxide and the corresponding cyclic carbonate (expect for 3,3-dimethyl-1,2-butene carbonate where the integral of the *t*Bu moieties was used).

Dimeric complex **4** displayed an even lower conversion of 43% for propylene oxide, but performed slightly better in the cases of styrene oxide (8%) and 1,2-epoxyhexane (11%) (entry 2). This can be ascribed to the smaller iPr groups of **4** (versus *t*Bu of **1**) in agreement with the observations made for magnesium pyrazolates.[20]

Scandium complex **7** performed best in this cycloaddition reaction, affording 99% conversion of propylene oxide with only traces of the starting material left (entry 3). Complex **7** also exhibited the highest catalytic activity of the metal pyrazolates under study for the three other epoxides, ranging from 24 to 29%. The yttrium-based catalysts **9** and **10** provided similar results, with monomeric **10** achieving slightly higher conversions than dimeric **9**, except for 1,2-epoxyhexane (entry 4 and 5). The results obtained for the cerium-based catalysts were in line with our earlier report, showing only slight deviations.[19] Strikingly, there seems to be a negative correlation between the carboxophilicity of the metal pyrazolate and its catalytic activity (Table 2). As described above, scandium carbamate **7-CO$_2$** releases CO_2 readily in the absence of a solvent or when placed in an open vessel. Also, under the applied conditions, mono-

Table 2 Correlation of catalytic conversion and CO_2 release temperatures (from VT ^{1}H NMR studies and TG measurements)

	CO_2-release temperature [°C]			
Catalyst	^{1}H NMR start → end	TGA start → end	Catalytic convers. [%]	Oxophilicity M [Θ][b]
15-Mg[a]	70–105	134–233	56	0.6
1-Al	100–120[c]	114–196	65	0.8
9-Y	rt–70	60–154	84	0.8
14-Ce^{IV}	10–60[a]	55–95[a]	88	0.9
13-Ce^{III}		52–90[a]	96	0.9
10-Y		—	97	0.8
7-Sc	rt	rt	>99	0.8

[a] Previous work Mg,[20] Ce.[19] [b] Ref. 84. [c] De-insertion not complete at this temperature, which is the upper limit of the VT NMR setup.

meric yttrium pyrazolate **10** did not insert any significant amount of CO_2, while dimeric yttrium pyrazolate **9** did insert CO_2 and displayed a CO_2-releasing step at 70 °C. Since the CO_2-release temperature range of complexes that reversibly insert CO_2 is an approximate measure of their carboxophilicity, comparison with the respective catalytic conversions clearly show that the lower the carboxophilicity, the higher the catalytic activity (Table 2). On the other hand, the carboxophilicity does not reflect the trends in the extent of the (calculated) oxophilicity (Table 2)[84] and electronegativity (Pauling scale)[85] and might be affected further by the Lewis acidity of the metal centre ($Al^{3+} > Sc^{3+} > Y^{3+}$), as well as the carbophilicity,[86] sterics and coordination mode (terminal *versus* bridging) of the carbamato ligand. For further comparison, the average N–C(CO_2) distance in complexes **1-Al-CO$_2$** (1.444(3) Å), **7-Sc-CO$_2$** (1.436(2) Å), $[Ce(CO_2{\cdot}pz^{Me_2})_3]_4$ (**13-CO$_2$**) (1.432(12) Å), $[Ce(CO_2{\cdot}pz^{Me_2})_4]$ (**14-CO$_2$** = **A**, Fig. 1 bottom) (1.436(3) Å) and $[Mg(CO_2{\cdot}pz^{tBu_2})_2(thf)_2]$ (**B**, Fig. 1 bottom) (1.477(1) Å) were detected in a close range.

Finally, the best-performing scandium complex **7** was examined for the cycloaddition of propylene oxide and CO_2 under varying conditions (Table 3). The aforementioned performance using the standard procedure (conversion of >99%) corresponds to a TON of >199 (entry 1). Decreasing the catalyst concentration to 0.25 mol% lowered the overall catalytic conversion to 71, but increased the TON to 284 (entry 2). Employing only 0.01 mol% of **7** at harsher reaction conditions (10 bar CO_2 and 90 °C), further increased the TON to 4600 (entry 3).

Table 3 Catalytic activity of **7** in the conversion of propylene oxide and CO_2 to cyclic carbonate under different conditions[a]

Entry	T [°C]/p[bar]	C (Cat.) [mol%]	Conversion[b] [%]	TON[c]
1	24/1	0.5	>99%	199
2	24/1	0.25	71%	284
3	90/10	0.01	45%	4600

[a] 24 h in neat epoxide. [b] Conversion determined by comparison of the integrals protons at the α-position of the epoxide and the corresponding cyclic carbonate. [c] ((epoxide/Mg) × conversion)/100.

The TOF of **7** was determined at 120 h^{-1} over the progress of the reaction applying our standard procedure (Fig. S86 and Table S1†).

Accordingly, complete conversion (>99%) was already detected after 12 h, but already after 6 h, the conversion was noted at 96%. Using half the amount of catalyst (entry 2) did not give similarly high conversions after 6 or 10 h, pointing to the catalyst load as the determining factor. Overall, a mechanism/catalytic cycle as described for the cerium and magnesium congeners is proposed.[19,20] To put the present catalytic results into a proper perspective, even the most active catalysts under study show only moderate catalytic activity in comparison to systems described in literature. For example, the chlorinated tetraphenyl porphyrin aluminium complex (tetra(2,4-chloro)phenylporphyrin)AlCl reaches TOFs of up to 185 200 h^{-1}.[36] For the rare-earth metals, the scorpionate complex $[La\{N(SiHMe_2)_2\}_2\{\kappa^3\text{-}(1\text{-}[2,2\text{-bis}(pz^{Me_2})\text{-}1,1\text{-}Ph_2Et]\text{-}1,3\text{-}Cp)\}]$ was noted at TOFs of 15 000 h^{-1} and TONs of up to 306 667.[57]

Conclusions

The scope and feasibility of reversible metal-pyrazolate CO_2-insertion chemistry is expandable to the trivalent light metals of groups 3 and 13. The reaction behaviors of monomeric aluminium(III) and scandium(III) pyrazolates are strikingly distinct under identical conditions. While homoleptic $Al(pz^{tBu_2})_3$, bearing the comparatively small metal centre, inserts two CO_2 molecules to form $Al(CO_2{\cdot}pz^{tBu_2})_2(pz^{tBu_2})$, $Sc(pz^{tBu_2})_3(thf)$ accommodates only one molecule CO_2 per scandium, affording the dimeric complex $[Sc(\mu\text{-}CO_2{\cdot}pz^{tBu_2})(pz^{tBu_2})_2]_2$. Both complexes feature completely reversible heteroallene insertion, as revealed by FTIR and VT ^{1}H NMR spectroscopy and thermogravimetric analysis (TGA). Again, strikingly, the aluminium complex releases the CO_2 only at temperatures >100 °C, while the scandium complex undergoes CO_2 de-insertion at ambient temperature and pressure. The implications of the pyrazolato substituents for the extent of CO_2 insertion was demonstrated for the new homoleptic complex $[Al(pz^{iPr_2})_3]_2$, which gave exhaustive CO_2 insertion, marking a capacity of 21.6 wt% CO_2. Applying the metal pyrazolates under study as catalysts in the cycloaddition of CO_2 and epoxides to cyclic carbonates revealed an inverse correlation of the catalytic activity and carboxophilicity (=CO_2 affinity): the higher the carboxophilicity, the lower the catalytic activity. Given the reversible CO_2 insertion into metal pyrazolates, the carboxophilicity can be assessed by the CO_2-release temperature (*via* VT ^{1}H NMR spectroscopy and TGA). The scandium complex $Sc(pz^{tBu_2})_3(thf)$ performed best, with a maximum TOF of 120 h^{-1} and a TON of 284 at ambient conditions.

Data availability

The data that support the findings of this study are available in the ESI† of this article.

Conflicts of interest

There are no conflicts of interest.

Acknowledgements

We are grateful to the VECTOR foundation (grant P2021-0099) for generous support. We thank Dr Markus Ströbele for running the TGA experiments.

References

1 S. Dhakal, J. C. Minx, F. L. Toth, A. Abdel-Aziz, M. J. Figueroa Meza, K. Hubacek, I. G. C. Jonckheere, Y.-G. Kim, G. F. Nemet, S. Pachauri, X. Tan and T. Wiedmann, *2022: Emissions Trends and Drivers. In IPCC, 2022: Climate Change 2022: Climate Change 2022: Mitigation of Climate Change. Contribution of Working Group III to the Sixth Assessment Report of the Intergovernmental Panel on Climate Change*, ed. P. R. Shukla, J. Skea, R. Slade, A. Al Khourdajie, R. van Diemen, D. McCollum, M. Pathak, S. Some, P. Vyas, R. Fradera, M. Belkacemi, A. Hasija, G. Lisboa, S. Luz and J. Malley, Cambridge University Press, Cambridge, UK and New York, NY, USA. DOI: 10.1017/9781009157926.004.

2 P. Falkowski, R. J. Scholes, E. Boyle, J. Canadell, D. Canfield, J. Elser, N. Gruber, K. Hibbard, P. Högberg, S. Linder, F. T. Mackenzie, B. Moore III, T. Pedersen, Y. Rosenthal, S. Seitzinger, V. Smetacek and W. Steffen, The Global Carbon Cycle: A Test of Our Knowledge of Earth as a System, *Science*, 2000, **290**, 291–296.

3 S. Solomon, G.-K. Plattner, R. Knutti and P. Friedlingstein, Irreversible climate change due to carbon dioxide emissions, *Proc. Natl. Acad. Sci. U. S. A.*, 2009, **106**, 1704–1709.

4 R. S. Haszeldine, Carbon Capture and Storage: How Green Can Black Be?, *Science*, 2009, **325**, 1647–1652.

5 D. W. Keith, Why Capture CO_2 from the Atmosphere?, *Science*, 2009, **325**, 1654–1655.

6 G. Centi and S. Perathoner, Opportunities and prospects in the chemical recycling of carbon dioxide to fuels, *Catal. Today*, 2009, **148**, 191–205.

7 M. Cokoja, C. Bruckmeier, B. Rieger, W. A. Herrmann and F. E. Kühn, Transformation of Carbon Dioxide with Homogeneous Transition-Metal Catalysts: A Molecular Solution to a Global Challenge?, *Angew. Chem., Int. Ed.*, 2011, **50**, 8510–8537.

8 N. von der Assen, P. Voll, M. Peters and A. Bardow, Life cycle assessment of CO_2 capture and utilization: a tutorial review, *Chem. Soc. Rev.*, 2014, **43**, 7982–7994.

9 M. Aresta, A. Dibenedetto and A. Angelini, Catalysis for the Valorization of Exhaust Carbon: from CO_2 to Chemicals, Materials, and Fuels. Technological Use of CO_2, *Chem. Rev.*, 2014, **114**, 1709–1742.

10 Q. Liu, L. Wu, R. Jackstell and M. Beller, Using carbon dioxide as a building block in organic synthesis, *Nat. Commun.*, 2015, **6**, 5933.

11 R. E. Siegel, S. Pattanayak and L. A. Berben, Reactive Capture of CO_2: Opportunities and Challenges, *ACS Catal.*, 2023, **13**, 766–784.

12 D. M. D'Alessandro, B. Smit and J. R. Long, Carbon Dioxide Capture: Prospects for New Materials, *Angew. Chem., Int. Ed.*, 2010, **49**, 6058–6082.

13 K. Sumida, D. L. Rogow, J. A. Mason, T. M. McDonald, E. D. Bloch, Z. R. Herm, T.-H. Bae and J. R. Long, Carbon Dioxide Capture in Metal–Organic Frameworks, *Chem. Rev.*, 2012, **112**, 724–781.

14 E. S. Sanz-Pérez, C. R. Murdock, S. A. Didas and C. W. Jones, Direct Capture of CO_2 from Ambient Air, *Chem. Rev.*, 2016, **116**, 11840–11876.

15 Y. Lin, C. Kong, Q. Zhang and L. Chen, Metal-Organic Frameworks for Carbon Dioxide Capture and Methane Storage, *Adv. Energy Mater.*, 2017, **7**, 1601296.

16 A. C. Forse and P. J. Milner, New chemistry for enhanced carbon capture: beyond ammonium carbamates, *Chem. Sci.*, 2021, **12**, 508–516.

17 J. Hack, N. Maeda and D. M. Meier, Review on CO_2 Capture Using Amine-Functionalized Materials, *ACS Omega*, 2022, **7**, 39520–39530.

18 R. Ayyappan, I. Abdalghani, R. C. Da Costa and G. R. Owen, Recent developments on the transformation of CO_2 utilising ligand cooperation and related strategies, *Dalton Trans.*, 2022, **51**, 11582–11611.

19 (*a*) U. Bayer, D. Werner, C. Maichle-Mössmer and R. Anwander, Effective and Reversible Carbon Dioxide Insertion into Cerium Pyrazolates, *Angew. Chem., Int. Ed.*, 2020, **59**, 5830–5836; (*b*) U. Bayer and R. Anwander, Carbonyl group and carbon dioxide activation by rare-earth-metal complexes, *Dalton Trans.*, 2020, **49**, 17472–17493.

20 F. Kracht, P. Rolser, P. Preisenberger, C. Maichle-Mössmer and R. Anwander, Organomagnesia: Reversibly High Carbon Dioxide Uptake by Magnesium Pyrazolates, *Adv. Sci.*, 2024, **11**, 2403295.

21 K. Ziegler, F. Krupp, K. Weyer and W. Larbig, Metallorganische Verbindungen, XLI Reaktionen der Aluminiumtrialkyle mit Kohlendioxyd und Schwefeldioxyd, *Justus Liebigs Ann. Chem.*, 1960, **629**, 251–256.

22 J. Weidlein, CO_2-Einschiebungsreaktionen bei Aluminium-, Gallium- und Indiumalkylverbindungen, *Z. Anorg. Allg. Chem.*, 1970, **378**, 245–262.

23 (*a*) D. B. Dell'Amico, F. Calderazzo, M. Dell'Innocenti, B. Guldenpfennig, S. Ilanelli, G. Pelizzi and P. Robino, N, N-Dialkylcarbamates of Silicon and Aluminium, *Gazz. Chim. Ital.*, 1993, **123**, 283–288; (*b*) D. B. Dell'Amico, F. Calderazzo, L. Labella, F. Marchetti and G. Pampaloni, Converting Carbon Dioxide into Carbamato Derivatives, *Chem. Rev.*, 2003, **103**, 3857–3897.

24 C.-C. Chang, B. Srinivas, W. Mung-Liang, C. Wen-Ho, M. Y. Chiang and H. Chung-Sheng, Fixation of CO_2 by a

Series of Ethynyl-Bridged Polynuclear Aluminum-Magnesium Complexes. Synthesis, Characterization, and Crystal Structures of $[Me_2Al(\mu\text{-}i\text{-}Pr_2N)_2Mg(\mu\text{-}C{\equiv}CR)]_2$ (R = C_6H_5, C_6H_4-p-CH_3, *t*-Bu, $SiMe_3$), $[Me_2Al(\mu\text{-}Et_2N)_2Mg(\mu\text{-}C{\equiv}CC_6H_5)]_2$, $\{(Me_2Al)_2[\mu\text{-}OO\text{-}C(i\text{-}Pr_2N)]_2\}$, and $\{(Me_2Al)_2[(\mu\text{-}OOC(i\text{-}Pr_2N))_2]_2Mg\}$, *Organometallics*, 1995, **14**, 5150–5159.

25 T. W. Yokley, H. Tupkar, N. D. Schley, N. J. DeYonker and T. P. Brewster, CO*2* Capture by 2-(Methylamino)pyridine Ligated Aluminum Alkyl Complexes, *Eur. J. Inorg. Chem.*, 2020, **2020**, 2958–2967.

26 For more reccent examples of CO_2 insertion into Al-pnictogenyl moieties, see: (*a*) W. Haider, M. D. Calvin-Brown, I.-A. Bischoff, V. Huch, B. Morgenstern, C. Müller, T. Sergeieva, D. M. Andrada and A. Schäfer, Diarylpnictogenyldialkylalanes – Synthesis, Structures, Bonding Analysis, and CO_2 Capture, *Inorg. Chem.*, 2022, **61**, 1672–1684; (*b*) E. Schumann, E. Brendler, U. Böhme and F. Mertens, Synthesis of Aluminum N,N-Dialkylcarbamates by Insertion of CO_2 into Al–N Bonds, *Eur. J. Inorg. Chem.*, 2023, **26**, e202200568.

27 P. Federmann, R. Müller, F. Beckmann, C. Lau, B. Cula, M. Kaupp and C. Limberg, Synthesis of Intramolecular P/Al-Based Frustrated Lewis Pairs via Aluminum-Tin-Exchange and their Reactivity toward CO_2, *Chem. – Eur. J.*, 2022, **28**, e202200404.

28 N. Takeda and S. Inoue, Activation of Carbon Dioxide by Tetraphenylporphinatoaluminium Methoxide. Reaction with Epoxide, *Bull. Chem. Soc. Jpn.*, 1978, **51**, 3564–3567.

29 T. Aida and S. Inoue, Activation of carbon dioxide with aluminum porphyrin and reaction with epoxide. Studies on (tetraphenylporphinato)aluminum alkoxide having a long oxyalkylene chain as the alkoxide group, *J. Am. Chem. Soc.*, 1983, **105**, 1304–1309.

30 F. Kojima, T. Aida and S. Inoue, Fixation and activation of carbon dioxide on aluminum porphyrin. Catalytic formation of a carbamic ester from carbon dioxide, amine, and epoxide, *J. Am. Chem. Soc.*, 1986, **108**, 391–395.

31 D. J. Darensbourg and M. W. Holtcamp, Catalysts for the reactions of epoxides and carbon dioxide, *Coord. Chem. Rev.*, 1996, **153**, 155–174.

32 M. Alvaro, C. Baleizao, E. Carbonell, M. El Ghoul, H. García and B. Gigante, Polymer-bound aluminium salen complex as reusable catalysts for CO_2 insertion into epoxides, *Tetrahedron*, 2005, **61**, 12131–12139.

33 D. Tian, B. Liu, Q. Gan, H. Li and D. J. Darensbourg, Formation of Cyclic Carbonates from Carbon Dioxide and Epoxides Coupling Reactions Efficiently Catalyzed by Robust, Recyclable One-Component Aluminum-Salen Complexes, *ACS Catal.*, 2012, **2**, 2029–2035.

34 C. J. Whiteoak, N. Kielland, V. Laserna, E. C. Escudero-Adán, E. Martin and A. W. Kleij, A Powerful Aluminum Catalyst for the Synthesis of Highly Functional Organic Carbonates, *J. Am. Chem. Soc.*, 2013, **135**, 1228–1231.

35 C. J. Whiteoak, N. Kielland, V. Laserna, F. Castro-Gómez, E. Martin, E. C. Escudero-Adán, C. Bo and A. W. Kleij, Highly Active Aluminium Catalysts for the Formation of Organic Carbonates from CO_2 and Oxiranes, *Chem. – Eur. J.*, 2014, **20**, 2264–2275.

36 Y. Qin, H. Guo, X. Sheng, X. Wang and F. Wang, An aluminum porphyrin complex with high activity and selectivity for cyclic carbonate synthesis, *Green Chem.*, 2015, **17**, 2853–2858.

37 M. A. St. Clair and B. D. Santarsiero, Structure of a scandium–carboxylate complex: $(\eta^5\text{-}C_5Me_5)_2Sc(O_2C)C_6H_4CH_3$, *Acta Crystallogr., Sect. C: Cryst. Struct. Commun.*, 1989, **45**, 850–852.

38 H. Schumann, J. A. Meese-Marktscheffel, A. Dietrich and F. H. Görlitz, Metallorganische Verbindungen der Lanthanoide: LXX. Bis(cyclopentadienyl)seltenerdkomplexe: Synthese und Röntgen-strukturanalyse von dem intramolekular stabilisierten Lutetiumalkyl $Cp_2Lu(CH_2)_3NMe_2$ und dem monomeren basenfreien Yttriumcarboxylat $Cp_2Y[\eta^2\text{-}O_2C(CH_2)_3NMe_2]$, *J. Organomet. Chem.*, 1992, **430**, 299–315.

39 W. J. Evans, C. A. Seibel, J. W. Ziller and R. J. Doedens, CO_2 Insertion Chemistry as a Probe of Organosamarium Allyl Reactivity, *Organometallics*, 1998, **17**, 2103–2112.

40 F. A. LeBlanc, A. Berkefeld, W. E. Piers and M. Parvez, Reactivity of Scandium β-Diketiminate Alkyl Complexes with Carbon Dioxide, *Organometallics*, 2012, **31**, 810–818.

41 O. T. Summerscales, C. M. Moore, B. L. Scott, M. P. Wilkerson and A. D. Sutton, Cerium(III) Carbonate Formation from $\{CeCp^*_2H\}_2$ and Carbon Dioxide: Structure and Mechanistic Insights, *Organometallics*, 2017, **36**, 4682–4685.

42 D. W. Beh, W. E. Piers, I. del Rosal, L. Maron, B. S. Gelfand, C. Gendy and J.-B. Lin, Scandium alkyl and hydride complexes supported by a pentadentate diborate ligand: reactions with CO_2 and N_2O, *Dalton Trans.*, 2018, **47**, 13680–13688.

43 D. Cui, M. Nishiura, O. Tardif and Z. Hou, Rare-Earth-Metal Mixed Hydride/Aryloxide Complexes Bearing Mono(cyclopentadienyl) Ligands. Synthesis, CO_2 Fixation, and Catalysis on Copolymerization of CO_2 with Cyclohexene Oxide, *Organometallics*, 2008, **27**, 2428–2435.

44 L. A. M. Steele, T. J. Boyle, R. A. Kemp and C. Moore, The selective insertion of carbon dioxide into a lanthanide(III) 2,6-di-*t*-butyl-phenoxide bond, *Polyhedron*, 2012, **42**, 258–264.

45 M. N. Bochkarev, E. A. Fedorova, Yu. F. Radkov, S. Ya. Khorshev, G. S. Kalinina and G. A. Razuvaev, Carbon dioxide fixaion by lathanide complexes, *J. Organomet. Chem.*, 1983, **258**, C29–C33.

46 Y. F. Rad'kov, E. A. Fedorova, S. Y. Khorshev, G. S. Kalinina, M. N. Bochkarev and G. A. Razuvaev, Reactions of carbon dioxide with bis(trimethylsilyl)amino derivatives of lanthanides, *Zh. Obshch. Khim.*, 1986, **56**, 386–389.

47 W. J. Evans, C. H. Fujimoto and J. W. Ziller, Organolanthanide-Based Coordination and Insertion Reactivity of the Anion Formed by Deprotonation of ε-Caprolactam, *Organometallics*, 2001, **20**, 4529–4536.

48 H. Yin, P. J. Carroll and E. J. Schelter, Reactions of a cerium(III) amide with heteroallenes: insertion, silyl-migration and de-insertion, *Chem. Commun.*, 2016, **52**, 9813–9816.

49 D. V. Vitanova, F. Hampel and K. C. Hultzsch, Rare earth metal complexes based on β-diketiminato and novel linked bis(β-diketiminato) ligands: Synthesis, structural characterization and catalytic application in epoxide/CO_2-copolymerization, *J. Organomet. Chem.*, 2005, **690**, 5182–5197.

50 D. Cui, M. Nishiura and Z. Hou, Alternating Copolymerization of Cyclohexene Oxide and Carbon Dioxide Catalyzed by Organo Rare Earth Metal Complexes, *Macromolecules*, 2005, **38**, 4089–4095.

51 A. Decortes, R. M. Haak, C. Martín, M. M. Belmonte, E. Martin, J. Benet-Buchholz and A. W. Kleij, Copolymerization of CO_2 and Cyclohexene Oxide Mediated by Yb(salen)-Based Complexes, *Macromolecules*, 2015, **48**, 8197–8207.

52 B. Xu, P. Wang, M. Lv, D. Yuan and Y. Yao, Transformation of Carbon Dioxide into Oxazolidinones and Cyclic Carbonates Catalyzed by Rare-Earth-Metal Phenolates, *ChemCatChem*, 2016, **8**, 2466–2471.

53 H. Yasuda, L.-N. He and T. Sakakura, Cyclic Carbonate Synthesis from Supercritical Carbon Dioxide and Epoxide over Lanthanide Oxychloride, *J. Catal.*, 2002, **209**, 547–550.

54 A. Ion, V. Parvulescu, P. Jacobs and D. de Vos, Sc and Zn-catalyzed synthesis of cyclic carbonates from CO_2 and epoxides, *Appl. Catal., A*, 2009, **363**, 40–44.

55 J. Qin, P. Wang, Q. Li, Y. Zhang, D. Yuan and Y. Yao, Catalytic production of cyclic carbonates mediated by lanthanide phenolates under mild conditions, *Chem. Commun.*, 2014, **50**, 10952–10955.

56 C. Wang, X. Liu, Z. Dai, Y. Sun, N. Tang and J. Wu, Yttrium complex supported by a sterically encumbering N-anchored tris-arylphenoxide ligand: Heteroselective ROP of rac-lactide and CO_2/epoxide coupling, *Inorg. Chem. Commun.*, 2015, **56**, 69–72.

57 J. Martínez, J. Fernández-Baeza, L. F. Sánchez-Barba, J. A. Castro-Osma, A. Lara-Sánchez and A. Otero, An Efficient and Versatile Lanthanum Heteroscorpionate Catalyst for Carbon Dioxide Fixation into Cyclic Carbonates, *ChemSusChem*, 2017, **10**, 2886–2890.

58 Z. Zhao, J. Qin, C. Zhang, Y. Wang, D. Yuan and Y. Yao, Recyclable Single-Component Rare-Earth Metal Catalysts for Cycloaddition of CO_2 and Epoxides at Atmospheric Pressure, *Inorg. Chem.*, 2017, **56**, 4568–4575.

59 O. Sodpiban, S. D. Gobbo, S. Barman, V. Aomchad, P. Kidkhunthod, S. Ould-Chikh, A. Poater, V. D'Elia and J.-M. Basset, Synthesis of well-defined yttrium-based Lewis acids by capturing a reaction intermediate and catalytic application for cycloaddition of CO_2 to epoxides under atmospheric pressure, *Catal. Sci. Technol.*, 2019, **9**, 6152–6165.

60 D. Pfeiffer, B. J. Ximba, L. M. Liable-Sands, A. L. Rheingold, M. J. Heeg, D. M. Coleman, H. B. Schlegel, T. F. Kuech and C. H. Winter, Synthesis, Structure, and Molecular Orbital Studies of Yttrium, Erbium, and Lutetium Complexes Bearing η^2-Pyrazolato Ligands: Development of a New Class of Precursors for Doping Semiconductors, *Inorg. Chem.*, 1999, **38**, 4539–4548.

61 G. B. Deacon, A. Gitlits, P. W. Roesky, M. R. Bürgstein, K. C. Lim, B. W. Skelton and A. H. White, Simple Syntheses, Structural Diversity, and Tishchenko Reaction Catalysis of Neutral Homoleptic Rare Earth(II or III) 3,5-Di-*tert*-butylpyrazolates—The Structures of $[Sc(t,Bu_2pz)_3]$, $[Ln_2(tBu_2pz)_6]$ (Ln=La, Nd, Yb, Lu), and $[Eu_4(tBu_2pz)_8]$, *Chem. – Eur. J.*, 2001, **7**, 127–138.

62 X. Zhou, L. Zhang, R. Ruan, L. Zhang, R. Cai and L. Weng, Synthesis of $[(C_5H_5Y(\eta^2\text{-}PzMe_2)(\eta\text{-}PzMe_2)]_2$ and $[Y(\eta^2\text{-}PzMe_2)_2(\eta\text{-}PzMe_2)(\eta\text{-}THF)]_2$ and the insertion of Me_2SiO into the Y-N bond, *Chin. Sci. Bull.*, 2001, **46**, 723–726.

63 D. Werner, G. B. Deacon, P. C. Junk and R. Anwander, Pyrazolates advance cerium chemistry: a CeIII/CeIV redox equilibrium with benzoquinone, *Dalton Trans.*, 2017, **46**, 6265–6277.

64 N. E. Rad, P. C. Junk, G. B. Deacon and J. Wang, New Homoleptic Rare Earth 3,5-Diphenylpyrazolates and 3,5-Di-*tert*-butylpyrazolates and a Noteworthy Structural Discontinuity, *Z. Anorg. Allg. Chem.*, 2019, **645**, 877–881.

65 G. B. Deacon, E. E. Delbridge, C. M. Forsyth, P. C. Junk, B. W. Skelton and A. H. White, Main Group Pyrazolates—the X-Ray Structures of $[Al(\eta^2\text{-}But_2pz)_3]$, $[SnMe_3(\eta^1\text{-}Ph_2pz)]$ and $[GePh_3(\eta^1\text{-}But_2pz)]$ (R_2pz = 3,5-Disubstituted Pyrazolate), *Aust. J. Chem.*, 1999, **52**, 733–740.

66 J. Lewiński, J. Zachara, P. Goś, E. Grabska, T. Kopeć, I. Madura, W. Marciniak and I. Prowotorow, Reactivity of Various Four-Coordinate Aluminum Alkyls towards Dioxygen: Evidence for Spatial Requirements in the Insertion of an Oxygen Molecule into the Al–C Bond, *Chem. – Eur. J.*, 2000, **6**, 3215–3227.

67 S. R. Kosuru, T.-H. Sun, L.-F. Wang, J. K. Vandavasi, W.-Y. Lu, Y.-C. Lai, S. C. N. Hsu, M. Y. Chiang and H.-Y. Chen, Enhanced Catalytic Activity of Aluminum Complexes for the Ring-Opening Polymerization of ε-Caprolactone, *Inorg. Chem.*, 2017, **56**, 7998–8006.

68 C.-C. Chang, T.-Y. Her, F.-Y. Hsieh, C.-Y. Yang, M. Y. Chiang, G.-H. Lee, Y. Wang and S.-M. Peng, Chemical Reactivities of $[Me_2AI(\mu\text{-}NiPr_2)_2MgMe]_4$ and $[Me_2AI(\mu\text{-}NiPr_2)_2MgCI]_2$: Crystal Structures of $[Me_2AI(\mu\text{-}Pz)_2AIMe_2]$, $[Me_2AI(\mu\text{-}Pz)_2Mg(\mu\text{-}Pz)_2AIMe_2]$, and $[Me_2Al(\mu\text{-}NiPr_2)(\mu\text{-}Me)Mg(\mu\text{-}NiPr_2)(\mu\text{-}Me)AIMe_2]$, *J. Chin. Chem. Soc.*, 1994, **41**, 783–789.

69 W. Zheng, H. Hohmeister, N. C. Mösch-Zanetti, H. W. Roesky, M. Noltemeyer and H.-G. Schmidt, Syntheses and Characterization of μ,η^1,η^1-3,5-Di-*tert*-butylpyrazolato Derivatives of Aluminum, *Inorg. Chem.*, 2001, **40**, 2363–2367.

70 N. E. Rad, P. C. Junk, G. B. Deacon, I. V. Taidakov, J. Wang, N. E. Rad, P. C. Junk, G. B. Deacon, I. V. Taidakov and J. Wang, Synthesis and Structural Characterisation of Lithium, Zinc, and Aluminium Pyrazolate Complexes*, *Aust. J. Chem.*, 2020, **73**, 520–528.

71 S. A. Cortes-Llamas and M.-Á. Muñoz-Hernández, Sodium Polypyrazolylaluminates: Synthesis, Characterization, and Isolation of a Reaction Intermediate of a Trispyrazolylaluminate, *Organometallics*, 2007, **26**, 6844–6851.

72 C. J. Snyder, M. J. Heeg and C. H. Winter, Poly(pyrazolyl) aluminate Complexes Containing Aluminum–Hydrogen Bonds, *Inorg. Chem.*, 2011, **50**, 9210–9212.

73 D. Sambade and G. Parkin, Synthesis and structural characterization of tris(pyrazolyl)hydroaluminate and tris(pyrazolyl)hydrogallate lithium compounds, *Polyhedron*, 2017, **125**, 219–229.

74 O. J. Garcia, L. Vendier, M. Etienne, S. Gwaltney, A. Ressler and M.-Á. Muñoz-Hernández, Cyclooctadiene Rh(I) Bis- and Tris(pyrazolyl)aluminate Complexes and Their Catalytic Activity on the Polymerization of Phenylacetylene, *Inorg. Chem.*, 2021, **60**, 10757–10763.

75 S. R. Kosuru, F.-J. Lai, Y.-L. Chang, C.-Y. Li, Y.-C. Lai, S. Ding, K.-H. Wu, H.-Y. Chen and Y.-H. Lo, Collaboration between Trinuclear Aluminum Complexes Bearing Bipyrazoles in the Ring-Opening Polymerization of ε-Caprolactone, *Inorg. Chem.*, 2021, **60**, 10535–10549.

76 B. M. Louie, S. J. Rettig, A. Storr and J. Trotter, Synthesis and crystal structure of tri(μ-carbonyl)bis[methyltris(1-pyrazolyl)gallato]dirhodium – benzene (1:1), *Can. J. Chem.*, 1984, **62**, 633–643.

77 G. A. Banta, B. M. Louie, E. Onyiriuka, S. J. Rettig and A. Storr, Synthesis and characterization of $LMo(CO)_3M(PPh_3)_x$ (where L = tridentate pyrazolyl-gallate or -borate ligand; M = Rh, $x = 2$; M = Cu, $x = 1$). X-ray crystal structures of $[MeGapz_3]Mo(CO)_3Rh(PPh_3)_2$ and $[MeGapz_3]Mo(CO)_3Cu(PPh_3)$ (where pz = pyrazolyl, $N_2C_3H_3$), *Can. J. Chem.*, 1986, **64**, 373–386.

78 E. C. Onyiriuka, S. J. Rettig and A. Storr, Synthesis and characterization of molybdenum–tin complexes derived from the molybdenum tricarbonyl anion, $[MeGapz_3]Mo(CO)_3^-$, and organotin chlorides. X-ray crystal structure of $[MeGapz_3]Mo(CO)_3SnPh_3$ (where pz = pyrazolyl, $N_2C_3H_3$), *Can. J. Chem.*, 1986, **64**, 321–327.

79 A. Frazer, B. Piggott, M. Harman, M. Mazid and M. B. Hursthouse, Syntheses and X-ray crystal structures of [bis{(3,5-dimethylpyrazolyl)$_3$hydridoborato}In]I and [bis{(pyrazolyl)$_3$methylgallato}In][InI_4], *Polyhedron*, 1992, **11**, 3013–3017.

80 S. N. König, G. Gerstberger, C. Schädle, C. Maichle-Mössmer, E. Herdtweck and R. Anwander, Unusual reaction pathways of gallium(III) silylamide complexes, *Main Group Met. Chem.*, 2013, **36**, 169–180.

81 (*a*) M. J. Heeg, Z. Yu and C. H. Winter, CCDC 781781: Experimental Crystal Structure Determination, 2011; (*b*) C. T. Sirimanne, W. Zheng, Z. Yu, M. J. Heeg and C. H. Winter, Synthesis, Structure, and Bridge-Terminal Exchange Kinetics of Pyrazolate-Bridged Digallium and Diindium Complexes Containing Bridging Phenyl Groups, *Organometallics*, 2005, **24**, 6184–6193.

82 For Ln_3Na_2 pyrazolate clusters with interstitial oxy ions, see: H. Schumann, P. R. Lee and J. Loebel, *Angew. Chem., Int. Ed. Engl.*, 1989, **28**, 1033–1035.

83 U. Bayer, A. Jenner, J. Riedmaier, C. Maichle-Mössmer and R. Anwander, Effect of Substituents of Cerium Pyrazolates and Pyrrolates on Carbon Dioxide Activation, *Molecules*, 2021, **26**, 1957.

84 (*a*) K. P. Kepp, A Quantitative Scale of Oxophilicity and Thiophilicity, *Inorg. Chem.*, 2016, **55**, 9461–9470; (*b*) K. A. Moltved and K. P. Kepp, The Chemical Bond between Transition Metals and Oxygen: Electronegativity, d-Orbital Effects, and Oxophilicity as Descriptors of Metal–Oxygen Interactions, *J. Phys. Chem. C*, 2019, **123**, 18432–18444.

85 L. Pauling, The Nature of the Chemical Bond. IV. The Energy of Single Bonds and the relative Electronegativity of Atoms, *J. Am. Chem. Soc.*, 1932, **54**, 3570–3582.

86 G. O. Kayode and M. M. Montemore, Factors controlling oxophilicity and carbophilicity of transition metals and main group metals, *J. Mater. Chem. A*, 2021, **9**, 22325–22333.